WDM-Compatible Polarization-Diverse OAM Generator and Multiplexer in Silicon Photonics

Yuxuan Chen, Zhongjin Lin, Simon Bélanger-de Villers, Leslie A. Rusch, and Wei Shi

IEEE Journal of Selected Topics in Quantum Electronics, (2019)

Doi: 10.1109/JSTQE.2019.2941488

https://ieeexplore.ieee.org/document/8839168

WDM-Compatible Polarization-Diverse OAM Generator and Multiplexer in Silicon Photonics

Yuxuan Chen, Zhongjin Lin, Simon Bélanger-de Villers, Leslie A. Rusch, *Fellow, IEEE,* and Wei Shi, *Member, IEEE*

***Abstract*—Spatial multiplexing using orbital angular momentum (OAM) modes is an efficient means of scaling up the capacity of fiber-optic communications systems; integrated multiplexers are crucial enablers of this approach. OAM modes are circularly polarized when propagating in a fiber, however, OAM generators previously demonstrated in silicon photonics use locally linearly polarized emitters. Coupling from multiplexers to fibers in those solutions results in extra loss and complexity. Moreover, many of those solutions are based on resonator structures with strong wavelength dependence, and are thus incompatible with wavelength-division multiplexing (WDM). We experimentally demonstrate on-chip generation and multiplexing of OAM modes using an array of circularly polarized 2D antennas with wide wavelength coverage. The proposed device was implemented on the standard 220-nm silicon-on-insulator platform. Optical vortex beams with OAM orders ranging from -3 to +3 in both left and right circular polarization states were generated from the same aperture across a wavelength range of 1540 nm to 1557 nm. This device could serve as a multiplexer or demultiplexer for up to 12 information bearing channels coupling into an OAM fiber, and is compatible with WDM multiplexing as well.**

***Index Terms*—Silicon photonics, orbital angular momentum, space division multiplexing, wavelength-division multiplexing, integrated photonic circuits.**

I. Introduction

THE capacity of wavelength division multiplexing (WDM) systems is rapidly approaching the Shannon limit. Space division multiplexing (SDM) provides a scalable solution offering capacity gain linear in the number of spatial channels [1], [2]. Linearly polarized (LP) modes are used in most of the few mode fiber SDM systems, as these modes are easy-to-generate and well-studied. Their disadvantage lies in mode interactions: LP modes that have fiber eigenmodes in common suffer from large crosstalk after transmission in fiber. While multi-input multi-output (MIMO) processing can be used at the receiver side to undo the coupling effects occurring within the fiber, this adds to complexity [3], [4]. MIMO processing scales up as the square of the number of modes, while digital signal processing (DSP) for low crosstalk systems scales linearly. As orbital angular momentum (OAM) modes are formed with fiber eigenmodes with the same propagation constant, they are lower in crosstalk than LP modes. There are no eigenmodes shared across OAM modes. OAM can eliminate the burden of MIMO processing, and thus lower power consumption and system complexity [5].

OAM can be generated in free-space with spiral phase plates [6], spatial light modulators [7], metasurfaces [8][9], and q-plates [10]. However, these free-space OAM setups are mostly bulky and cumbersome. They are also vulnerable to even small changes in angle or position. Scaling to a large number of modes leads to a prohibitively complex system of parallel spatial paths.

Silicon photonics is a scalable technology for complex photonic integrated circuits (PICs). Ultra-compact OAM generators have been demonstrated on silicon [11]. In [12], heaters exploit the tunability of silicon to create a continuously tunable OAM generator. However, these devices are resonator based, in which the OAM order depends on the resonance wavelength. Therefore, they are not generally compatible with WDM.

Polarization properties of OAM generators impact their suitability for OAM destined to propagate in fiber where circular polarization is required. Most integrated OAM generators demonstrated so far use linearly polarized emitters. For example, the photonic circuit demonstrated in [12] are operated in TE polarization, where the optical emission from each emitter is azimuthally polarized. In [13], a 3D waveguide block converts the wavefront from a 1D silicon waveguide array to a 2D emitter in glass. There the OAM polarization is azimuthal if the TE waveguide mode is used, and radial if TM waveguide mode is used. As fiber OAM modes can only be circularly polarized, devices based on linearly-polarized emitters would need to convert the azimuthal or radial polarization into circular polarization for fiber propagation, resulting in excess loss and complexity.

We recently proposed a silicon PIC [14][15] for on-chip OAM generation and multiplexing in circular polarization designed for broad wavelength coverage. We use an array of 2D antennas as emitters. We use directional couplers to provide a 90-degree phase delay between the two antenna inputs for direct generation of circular polarized OAM beams. However, the device was only examined numerically (no experimental demonstration) and for 2D antenna number limited by targeting butt coupling to the OAM fiber.

In this paper, we revisit the design in [14] to increase the number 2D antennas, thereby increasing the resolution of OAM beams generated and accommodating higher order modes. Butt coupling could be replaced with a simple lens assembly to couple to the fiber. We fabricate the device and present experimental characterizations of this WDM-compatible, polarization-diverse OAM generator and multi-

The authors are with the Department of Electrical and Computer Engineering, Centre for Optics, Photonics and Lasers (COPL), University of Laval, Quebec, QC G1V 0A6, Canada (e-mail: yuxuan.chen.1@ulaval.ca; zhongjin.lin.1@ulaval.ca; simon.belanger-de-villers.1@ulaval.ca; leslie.rusch@gel.ulaval.ca; wei.shi@gel.ulaval.ca).

National Science and Engineering Research Council of Canada (NSERC) Funding: CRDPJ 515539-17

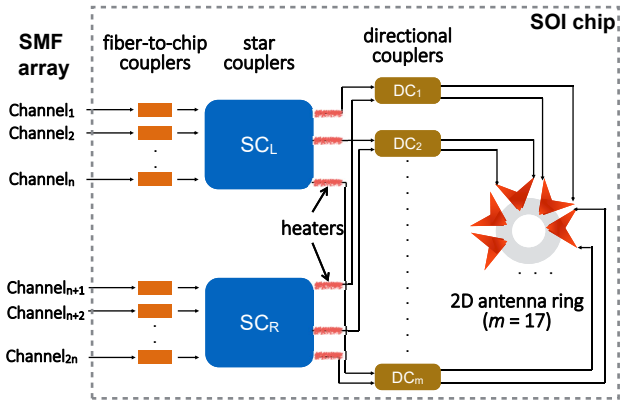

Fig. 1: Block diagram of the proposed integrated OAM generator/multiplexer.

plexer. Vortex beams with OAM orders ranging from -3 to 3 in both left and right polarization states, for 14 OAM modes in total, have been observed across a wide wavelength range. We discuss the practical considerations of our physical implementation in detail.

II. Chip Design and Fabrication

A block diagram of the proposed OAM generator and multiplexer device is shown in Fig. 1. On-chip fiber couplers allow a single mode fibre (SMF) array to input signals in a mux configuration, or to output signals in a demux configuration; we assume the mux configuration for our discussions. The chip inputs are denoted Channel_1 to Channel_{2n}, and they map to $2n$ unique OAM states at the mux output. Each output is distinguished by its polarization, topological charge and direction of rotation of the phase front. The polarization is either left circular polarization (LCP) or right circular polarization (RCP). Topological charge is an integer that denotes the number of rotations of the phase front. The direction of the rotation is the sign of topological charge; it can be positive or negative. Inputs are grouped into two sections: Channels 1 to n for LCP, and Channels $n+1$ to $2n$ for RCP. In this specific device, since OAM -3 to +3 were generated in each circular polarization, n equals to 7.

The fiber-to-chip couplers are followed by two identical star couplers. The upper one, denoted SC_L, is fed with input channels destined to have LCP. The one on the bottom, denoted SC_R, is fed with channels destined to have RCP. The star couplers do not manipulate polarization, but instead perform the task of tilting the phase front of the light from each input waveguide. The amount of tilt applied is varied with input waveguide position to obtain the desired mapping of input position to target output OAM state topological charge and direction of rotation. The position and width of the input and output waveguides, as well as the length of the free propagation region, are carefully adjusted to achieve appropriate phase difference between adjacent waveguides. Assuming only one input channel is activated, say one targeting LCP for example, we would ideally see light with equal amplitude and uniformly spaced phase at all outputs of SC_L, and no light at SC_R outputs.

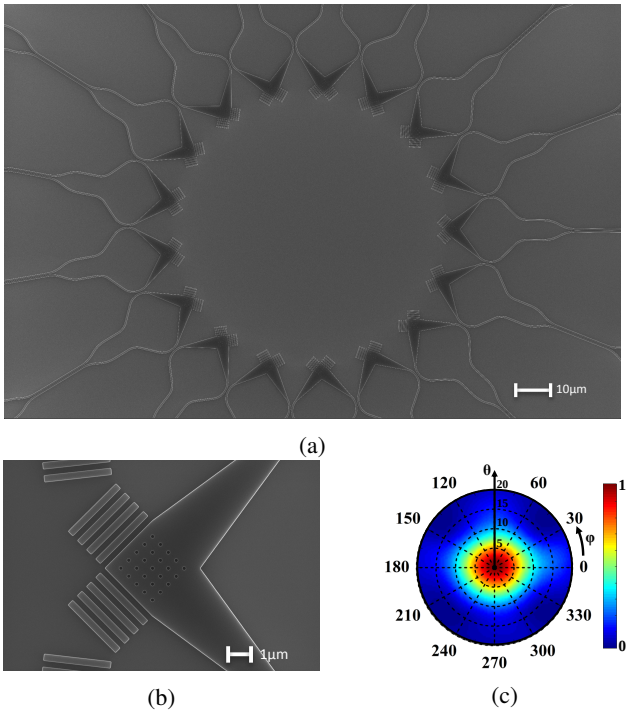

Fig. 2: (a) SEM image of the fabricated emitter section, (b) SEM image of a 2D antenna, and (c) simulated far field distribution of the 2D antenna .

Each SC_L output waveguide and its corresponding SC_R output are routed, respectively, to the upper and lower input ports of a directional coupler. By corresponding we mean with the same target topological charge and direction of rotation. The directional coupler (DC) consists of two strip waveguides with the identical geometry in the coupling region. The length of the coupling region is chosen to achieve a 50-50 splitting ratio at 1550 nm. At the end of the coupling regime, the DC introduces a 90-degree phase shift between the output ports; the shift is perceived as positive or negative depending on the input port. This phase delay is important for generation of circular polarization.

Each pair of outputs of one directional coupler is then combined via a 2D antenna. The phase difference between the outputs of directional coupler determines the polarization of the emitted vortex beam (LCP or RCP). They are analogous to a quarter-wave plate in functionality. By reversing the propagation direction of light, this device becomes a demultiplexer.

The proposed OAM generator/multiplexer was designed based on the 220-nm-thick silicon-on-insulator (SOI) wafer with a 2-μm-thick buried oxide layer. An array of 17 2D-antennas is used in the emitter section, as shown in Fig. 2a. The number 17 was chosen for a compromise between angular phase resolution and vulnerability to fabrication non-uniformity. The 2D antennas are designed for vertical emission so that the synthesized field achieves a well defined OAM wavefront [14]. The 2D grating region has a uniform pitch of 600nm in both axes, with a hole radius of 100nm. Four periods of Bragg gratings with a 695nm pitch and 50% filling factor are added after the square 2D grating region to improve

National Science and Engineering Research Council of Canada (NSERC) Funding: CRDPJ 515539-17

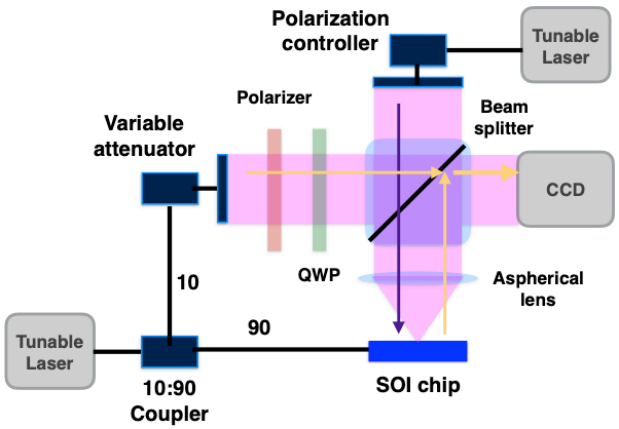

Fig. 3: Experimental setup to characterize chip and observe interference patterns.

the coupling efficiency. With these design parameters, the 2D antenna achieves 40% up-emitting efficiency and is well confined within an angle of 10 degree in the far field. The scanning electron microscope (SEM) image of a fabricated 2D antenna is shown in Fig. 2b, with its simulated far field distribution in Fig. 2c. The far field distribution was simulated using a numerical finite-difference time-domain solver.

To minimize phase errors, we place the directional couplers to the 2D antennas as close as possible, as shown in Fig. 2a. To maintain the relative phase difference created by the star couplers, we designed the waveguides so that they have the same length from SC_L/SC_R to the 2D antennas. We also deploy a metal heater to the top of each waveguide path for phase tuning. By applying voltage to the metal heaters, we can independently change the refractive index of each path to compensate phase errors during fabrication. The routing waveguides are placed 65 μm apart to avoid heat crosstalk from adjacent heaters.

The chip was fabricated using a rapid-prototyping electron-beam lithography (EBL) process at Applied Nanotools Inc. [16]. Surface grating couplers [17] were used for coupling between the silicon chip and the SMF array.

III. Experiment

We performed two steps of characterization in our experiment. The first characterization aimed at compensating the phase error induced in fabrication. To do so, we operated the chip in the de-multiplexing mode and found heater settings that minimized crosstalk. In the second characterization, we examined the chip in the multiplexing mode and confirmed generation of OAM modes by observing their characteristic interferograms.

A. Crosstalk characterization and phase error crrection

The characterization begins by launching a normal Gaussian beam (OAM0, i.e., the fundamental mode) onto the chip and observing the fiber array outputs. Our experimental setup is shown in Fig. 3, with the relevant sections for this characterization being the upper section and purple arrow for the light path. A polarization controller is used to convert the output of a tunable laser (top right in Fig. 3) to either LCP or RCP. We monitor the power on all demultiplexed outputs via the SMF array. For a fundamental mode in LCP, all the power should ideally go to the port that corresponds to zeroth order OAM LCP in the SMF array. Power found in other fiber ports is crosstalk to other OAM modes. We sweep the voltage applied on each metal heater from 2V to 6V until we find the optimum voltage, i.e., when we maximize the power at the zeroth order port. The phase correction for RCP is done following the same procedure.

Fig. 4 summarizes the crosstalk characterized with zeroth order OAM. The x-axis shows the OAM orders of the ports monitored for crosstalk, that is, the non-zeroth-order channels. The y-axis shows the crosstalk defined by the ratio of undesired output power to the input power. The red bars show the measure crosstalk for the chip as fabricated and not using any heaters to compensate for phase errors. For LCP, the worst case is the OAM+1 channel; for RCP, it is OAM-3. The worst crosstalk for both LCP and RCP is above 0 dB, which means more power were detected in a higher-order OAM channel than in the target zeroth-order OAM channel. Clearly the phase errors during fabrication are severe and cause excessive degradation of the sought-after constructive interference in the target channel.

The hollow bars in Fig. 4 represent the measured crosstalk after optimizing the heater voltages. With thermal tuning to correct the phase errors, we managed to significantly improve

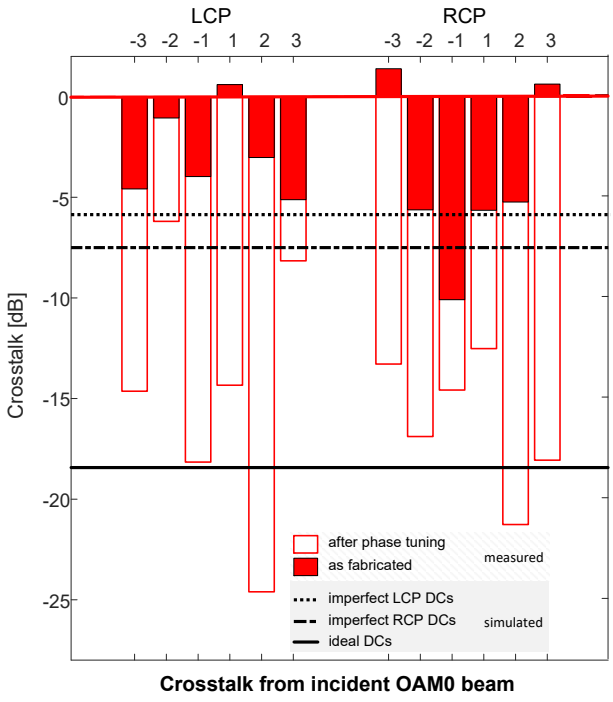

Fig. 4: Measured crosstalk for OAM0: as fabricated (red bar) and after phase tuning (hollow bar); simulated worst crosstalk with ideal 50-50 directional couplers (DCs) and minimum experimental phase resolution, as well as simulated worst case crosstalk for RCP and LCP with imperfect DCs.

National Science and Engineering Research Council of Canada (NSERC) Funding: CRDPJ 515539-17

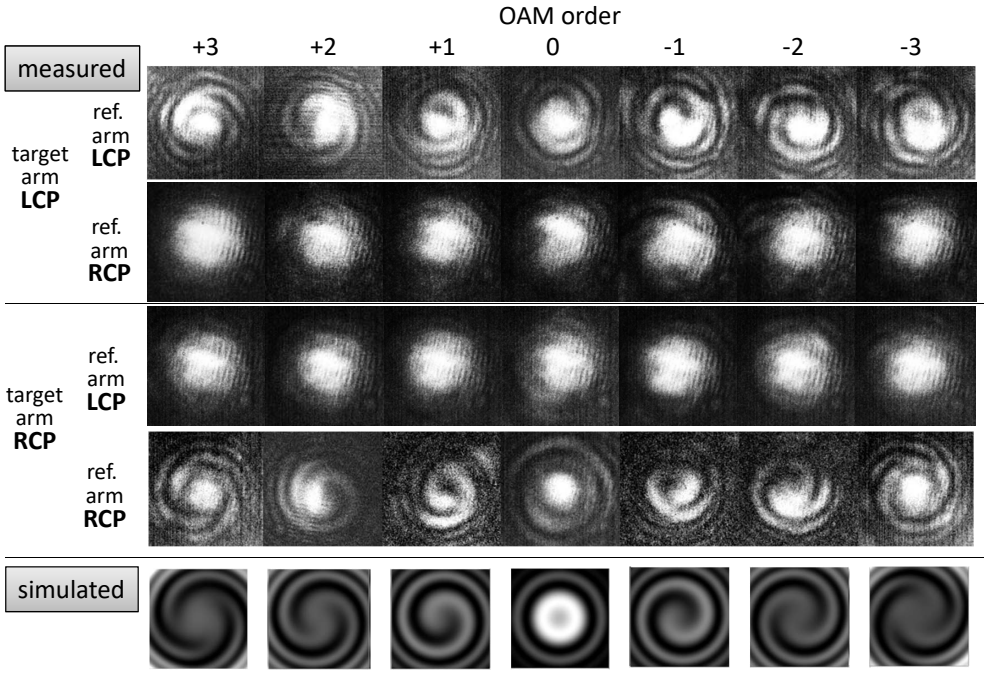

Fig. 5: Interferograms (OAM orders appear above columns) for: row 1) LCP generation with LCP reference, row 2) LCP generation with RCP reference, row 3) RCP generation with LCP reference, row 4) RCP generation with RCP reference, and row 5) simulated LCP generation with LCP reference.

the crosstalk; improvement in LCP channel 2 was 22 dB. The worst crosstalk was measured to be -6.20 dB for LCP, and -12.52 dB for RCP.

Assuming an ideal 50-50 power splitting ratio of the directional coupler (DC), we simulated our chip using the model presented in [14]. The worst case crosstalk was found to be around -18 dB (solid line in Fig. 4). The difference between the experimental measurements and the simulation prediction was large, as even after tuning the worst case was a distant -6 dB. The other horizontal line from simulation results are discussed in section IV.

During the experiment, we observed a sinusoidal variation in output power of the zeroth order port when sweeping the voltage. We sweep the heating voltage for one path at a time. As we continuously change the voltage applied on the waveguide being heated, we continuously change the phase in that waveguide. When functioning as a demultiplexer, the output power of the zeroth order port is the interference of all path. Thus, this sinusoidal trend intuitively reflects the continuous phase change in the heated waveguide. Three periods of sinusoidal variation were observed within a range of 2V to 6V. We varied the voltage by 0.04 V per step for a phase resolution of approximately 10.8 degree.

B. Validation of OAM via interferograms

The second characterization sends a signal to one fiber in the fiber array and observes an interferometric pattern generated from the chip output beam. Our experimental setup is again shown in Fig. 3, with the relevant sections for this characterization being the lower section and yellow arrows for light paths through the beam splitter. The tunable laser is now relocated to the fiber input, but first split into two paths. One path will serve as the reference Gaussian signal for the interferometer; the other path feeds the SOI chip to create the target signal. In this characterization, the SOI chip functions as an OAM generator. We fix the voltage applied on each metal heater to those optimal values found previously.

The beam from the laser is split at a ratio of 90:10, with 90% of its power coupled to the SOI chip (one channel a time) through the SMF array (Fig. 1). Polarization maintaining fibers are used to couple light to the TE waveguide mode. The beam emitted from the 2D-antenna array is collimated through an aspherical lens and then passes a non-polarization-sensitive beam splitter. The reference beam comes from the left side of the beam splitter. We measure the power from the chip output and use a variable attenuator to match reference signal power to the target signal power emitted from the chip. To observe the characteristic spiral interferograms, in the reference path we use a polarizer followed by a quarter wave plate to produce a circularly polarized reference beam. The reference beam and the chip-emitted OAM beam are combined by the beam splitter. Their interferograms are recorded using a CCD camera.

We activate one channel at a time. Each channel corresponds to a specific OAM state. We interfere each of generated OAM beams with the reference beam twice, once for each circular polarization of the reference beam. When the polarization states of the reference beam and the OAM beam align with each other, we expect to see characteristic spiral pattern in the interferogram with the number of nested spirals equal to the topological charge of the OAM state. For opposite polarization states, we expect to see a simple circular Gaussian-like

National Science and Engineering Research Council of Canada (NSERC) Funding: CRDPJ 515539-17

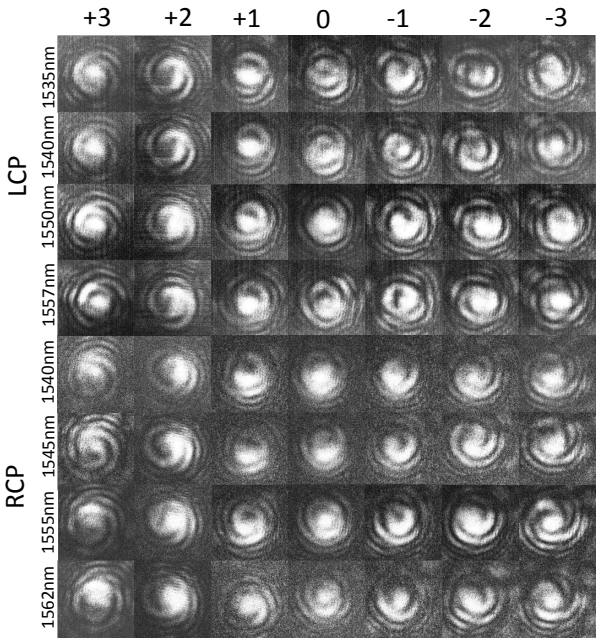

Fig. 6: Interferograms for target and reference beams with identical polarizations for various wavelengths; target OAM orders appear on the top, and polarization and wavelength are indicated to the left of each row.

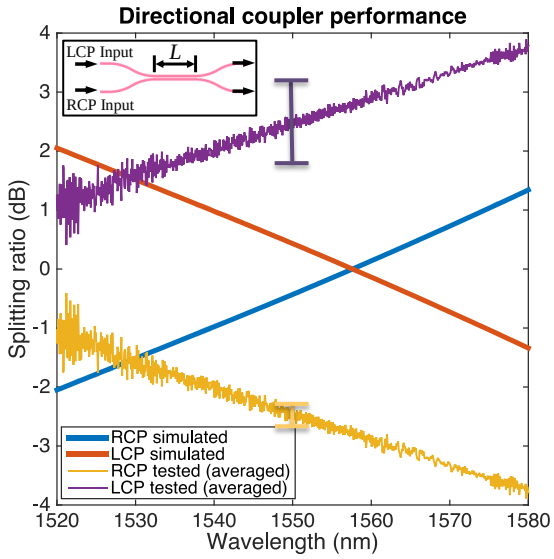

Fig. 7: Simulated and measured splitting ratios of the directional coupler. Solid lines: simulation; markers: measurement at 1550 nm of several devices with the same design fabricated on the same chip.

intensity pattern in the interferogram.

The measured interferograms at 1550nm are shown in Fig. 5. The intended OAM order (determined by input port) is indicated by the number at the top of each column. From Fig. 5, with opposite polarizations between target and reference, we observe circular Gaussian intensity profiles as expected. For all cases with aligned polarizations, we can clearly observe spiral patterns, confirming generation of OAM beams. The spiral patterns for RCP are in general of greater purity, as expected given the 6 dB difference in crosstalk levels between RCP and LCP in our characterization. The number of spirals observed in each of these interferograms matches with the target OAM states. For comparison, in the fifth row of Fig. 5, we show simulation results for LCP generation. RCP generation should ideally have the same performance in simulation.

C. Validation of WDM compatibility via interferograms

To demonstrate the WDM compatibility of our design, we repeated interferograms at swept wavelengths. We again fixed the voltage applied on each metal heater to those optimal values found previously. The results are shown in Fig. 6. The spiral patterns become less clear when the wavelength deviates from 1550 nm Fig. 5. The maximum and minimum wavelengths included in Fig. 6 represent the extremes we were able to cover. When we go beyond these extremes, the spirals in the 3rd order OAM become corrupted; the number of spirals no longer match with the topological charge. This is very likely due to the limited bandwidth of the star coupler and directional coupler. At beyond-extreme wavelengths, the phase assigned by star coupler is no longer appropriate for supporting 3rd order generation. Since the splitting ratio of directional coupler is highly non-uniform across these wavelengths, the power of the circularly polarization emission is lower.

The extreme wavelengths for LCP and RCP are offset by 5 nm. The overlapping region, 1540 nm to 1557 nm, represents the exploitable range of our chip. We can generate all 7 OAM modes in both circular polarizations over a 17 nm optical spectral range within the C-band, providing 14 OAM channels in free space and 12 OAM channels in an OAM fiber (since the LCP +1 order and RCP -1 order of OAM cannot steadily propagate in OAM fiber [18]).

IV. Discussion

As the schematic in Fig. 1 shows, our design is circularly symmetric for LCP generation and RCP generation. The waveguide routing lengths are also identical for both polarization states. Nonetheless, we observed a 5 nm offset (Fig. 6) in the operating wavelength range and around 6 dB difference Fig. 4 in crosstalk between LCP and RCP after the phase error correction. We attribute these differences between LCP and RCP performance to variations in the directional couplers. In our design and simulation, we have assumed a 50:50 splitting ratio, i.e., 0 dB if expressed in the log scale. Nevertheless, the directional coupler is wavelength dependent and sensitive to waveguide geometry variation due to fabrication errors. As we used 17 directional couplers in our device, the wafer non-uniformity and non-ideal lithography may add up significantly and result in a large variation in splitting ratio. This motivated a new set of simulations to predict the crosstalk measured in Fig. 4.

To parameterize our crosstalk simulations, we start by examining the directional coupler wavelength dependence. We experimentally examined multiple copies of the same directional coupler design placed at various locations of our

National Science and Engineering Research Council of Canada (NSERC) Funding: CRDPJ 515539-17

fabricated chip. The schematic of a directional coupler is shown in the inset in upper portion of Fig. 7. The length of the coupler is $L = 16$ μm. Figure 7 shows the splitting ratio of the directional coupler as function of wavelength. The two solid curves in the figure represent the simulated results of the directional coupler: the red curve for the LCP port, the blue curve for the RCP input port. We also present two sets of experimental data in Fig. 7. The magenta line is an average of measurements collected from the upper (LCP input injections) input to several directional couplers, and the yellow line is for the lower input (RCP). We measured the mean and standard deviation of our measurements across multiple devices. For the upper input port, which corresponds to LCP generation, the mean μ is 2.25 dB with a standard deviation σ of 1.15 dB at 1550 nm, while for RCP generation, the mean is -2.3 dB with a standard deviation of 0.4 dB.

This large variation in splitting ratio between upper and lower inputs leads, in two respects, to the differences observed in LCP and RCP generation. The variation results in power non-uniformity between LCP and RCP generation. A larger variation from the LCP input results in a lower power of LCP OAM beams compared to their RCP counterparts with the same OAM orders. The standard deviation relates to "purity" or crosstalk level of the generated beams. Having a larger standard deviation, the crosstalk of LCP OAM beams is also higher than their RCP counterparts, as shown in Fig. 5.

To quantify the impact of the splitting ratio errors introduced by fabrication imperfections, we simulated our device using the model that we proposed in [14]. Using this statistics (mean and variance) illustrated in Fig. 5, we modeled variation as a normal distribution. We randomly generated 1000 splitting ratios of directional couplers from this Gaussian distribution, assuming no phase error. From these calculations, the worst crosstalk is -5.86dB for LCP generation, and -7.79dB for RCP generation. These results are plotted in Fig. 4 and labeled as simulated worst case crosstalk for imperfect directional couplers. The dotted line were results for the LCP statistics, and the dashed line for RCP statistics. This result explains the performance difference between LCP and RCP. The statistics on splitting ratio leads to a crosstalk difference. This also accounts for the significant difference between the measured worst case crosstalk and the theoretically prediction (solid line in Fig. 5). Our experimental results after phase correction, shown in hollow bars in Fig. 4, are better than their predicted worst case. Hence our simulations explain the trend, but do not quantify the effect.

The strong wavelength dependence of the directional coupler most likely also limits the operational spectral range of the OAM multiplexer. In our future work, we will replace the directional coupler with a broadband 2×2 MMI (e.g., [19]) for a more robust design with significantly improved performance in polarization diversity and a larger wavelength range.

The total optical loss of this device is calibrated when functioning as a mux. For all 14 OAM channels, the loss ranges from 25dB to 26.7dB, including 7dB from the surface grating coupler, 5dB from the star couplers, 3dB waveguide loss and 10dB from 2D antenna ring. These losses can be improved from several perspectives: with dual etch steps, 1.2dB loss has been obtained from apodized surface grating coupler [20]; backside metal mirror has been proved to be able to increase the coupling efficiency as well [21], the loss for 2D antenna ring could potentially be reduced to 4dB according to our simulation; by optimizing the routing strategy, we could reduce the waveguide loss to around 2dB. These techniques can be implemented in our future work and reduce the total optical loss of the device to around 12dB.

V. Conclusion

We have demonstrated a chip-scale, WDM-compatible polarization-diverse OAM generator and multiplexer that supports up to third order OAM. We described our characterization methodology and how it could be used to thermally tune to correct for phase errors. Measured interferograms demonstrated OAM spirals of the desired chirality over 17 nm within the C-band. To the best of our knowledge, this is the first demonstration of directly generating and multiplexing circularly polarized OAM modes on a silicon chip, meeting the needs of a multiplexer for OAM fiber transmission.

Our device provides a scalable multiplexing solution. The design can accommodate more OAM channels by increasing the number of 2D antennas in the emitter section. Furthermore, as the device was fabricated using the standard 220-nm SOI process, it can be readily integrated with many other photonic components such as WDM filters [22], high-speed CMOS-photonics modulators [23], coherent transmitters [25][24], and Ge photo detectors [26] for ultra-high-capacity WDM $\times$ SDM transmission systems.

Acknowledgment

This work was supported by Huawei Canada and NSERC (CRDPJ 515539-17). We thank S. Levasseur and N. Bacon with Université Laval for their technical support. We also thank Drs. J. Lin, L. Wang and Z. Jiang with Huawei Canada for useful discussions.

References

[1] Winzer, Peter J., David T. Neilson, and Andrew R. Chraplyvy. "Fiber-optic transmission and networking: the previous 20 and the next 20 years." Optics express 26.18 (2018): 24190-24239.

[2] Winzer, Peter J., and David T. Neilson. "From scaling disparities to integrated parallelism: A decathlon for a decade." Journal of Lightwave Technology 35.5 (2017): 1099-1115.

[3] Randel, Sebastian, et al. "6 56-Gb/s mode-division multiplexed transmission over 33-km few-mode fiber enabled by 6 6 MIMO equalization." Optics Express 19.17 (2011): 16697-16707.

[4] Ryf, Roland, et al. "Mode-Division Multiplexing Over 96 km of Few-Mode Fiber Using Coherent 6×6 MIMO Processing." Journal of Lightwave technology 30.4 (2011): 521-531.

[5] Rusch, L.A., Rad, M., Allahverdyan, K., Fazal, I. and Bernier, E., 2018. Carrying data on the orbital angular momentum of light. IEEE Communications Magazine, 56(2), pp.219-224.

[6] Massari, M., Ruffato, G., Gintoli, M., Ricci, F. and Romanato, F., 2015. Fabrication and characterization of high-quality spiral phase plates for optical applications. Applied Optics, 54(13), pp.4077-4083.

[7] Ohtake, Y., Ando, T., Fukuchi, N., Matsumoto, N., Ito, H. and Hara, T., 2007. Universal generation of higher-order multiringed Laguerre-Gaussian beams by using a spatial light modulator. Optics letters, 32(11), pp.1411-1413.

[8] Lei, T., Zhang, M., Li, Y., Jia, P., Liu, G.N., Xu, X., Li, Z., Min, C., Lin, J., Yu, C. and Niu, H., 2015. Massive individual orbital angular momentum channels for multiplexing enabled by Dammann gratings. Light: Science & Applications, 4(3), p.e257.
[9] Li, Y., Li, X., Chen, L., Pu, M., Jin, J., Hong, M. and Luo, X., 2017. Orbital angular momentum multiplexing and demultiplexing by a single metasurface. Advanced Optical Materials, 5(2), p.1600502.
[10] Karimi, E., Piccirillo, B., Nagali, E., Marrucci, L. and Santamato, E., 2009. Efficient generation and sorting of orbital angular momentum eigenmodes of light by thermally tuned q-plates. Applied Physics Letters, 94(23), p.231124.
[11] Zhang, D., Feng, X. and Huang, Y., "Encoding and decoding of orbital angular momentum for wireless optical interconnects on chip," Optics Express, 2012, 20(24), pp. 26986-26995.
[12] Sun, J., Yaacobi, A., Moresco, M., et al., 2014, "Chip-scale continuously tunable optical orbital angular momentum generator", arXiv preprint arXiv:1408.3315.
[13] Guan, B., Qin, C., Scott, R.P., et al., October 2015, "Polarization diversified integrated circuits for orbital angular momentum multiplexing," in 2015 IEEE Photonics Conference (IPC), pp. 649-652.
[14] Chen, Y., Rusch, L.A. and Shi, W., 2018, "Integrated circularly polarized OAM generator and multiplexer for fiber transmission," IEEE Journal of Quantum Electronics, 54(2), pp. 1-9.
[15] Lin, Z., Chen, Y., Rusch, L. and Shi, W., 2018. On-Chip Circular Polarization Splitter Using Silicon Photonic Nanoantenna Array. ACS Photonics, 5(11), pp.4338-4342.
[16] L. Chrostowski, H. Shoman, M. Hammood et al., "Silicon Photonic Circuit Design Using Rapid Prototyping Foundry Process Design Kits," IEEE Journal of Selected Topics in Quantum Electronics, 2019.
[17] Yun Wang, Xu Wang, Jonas Flueckiger, et al., "Focusing sub-wavelength grating couplers with low back reflections for rapid prototyping of silicon photonic circuits," Opt. Express 22, 20652-20662 (2014).
[18] Brunet, C., Vaity, P., Messaddeq, Y., LaRochelle, S. and Rusch, L.A., 2014. Design, fabrication and validation of an OAM fiber supporting 36 states. Optics express, 22(21), pp.26117-26127.
[19] Guan, Hang, et al. "Compact and low loss 90 optical hybrid on a silicon-on-insulator platform." Optics Express 25.23 (2017): 28957-28968.
[20] Chen, X., Li, C., Fung, C.K., Lo, S.M. and Tsang, H.K., 2010. Apodized waveguide grating couplers for efficient coupling to optical fibers. IEEE Photonics Technology Letters, 22(15), pp.1156-1158.
[21] Van Laere, F., Roelkens, G., Ayre, M., Schrauwen, J., Taillaert, D., Van Thourhout, D., Krauss, T.F. and Baets, R., 2007. Compact and highly efficient grating couplers between optical fiber and nanophotonic waveguides. Journal of lightwave technology, 25(1), pp.151-156.
[22] Shi, Wei, et al. "Ultra-compact, flat-top demultiplexer using anti-reflection contra-directional couplers for CWDM networks on silicon." Optics express 21.6 (2013): 6733-6738.
[23] Sepehrian, Hassan, et al. "CMOS-photonics codesign of an integrated DAC-less PAM-4 silicon photonic transmitter." IEEE Transactions on Circuits and Systems I: Regular Papers 63.12 (2016): 2158-2168.
[24] Lin, J., Sepehrian, H., Rusch, L. A., and Shi, W. (2019). Single-carrier 72 GBaud 32QAM and 84 GBaud 16QAM transmission using a SiP IQ modulator with joint digital-optical pre-compensation. Optics express, 27(4), 5610-5619.
[25] Hassan Sepehrian, Jiachuan Lin, Leslie Ann Rusch, and Wei Shi, "Silicon Photonic IQ Modulators for 400 Gb/s and Beyond," J. Lightwave Technol. 37, 3078-3086 (2019)
[26] Zhang, Yi, et al. "A high-responsivity photodetector absent metal-germanium direct contact." Optics express 22.9 (2014): 11367-11375.

Yuxuan Chen was born in Wuhan, China, in 1992. He received his B.S. degree in Opto-Information Science and Technology from Huazhong University of Science and Technology, Wuhan, China in 2014. He is currently working toward his Ph.D. degree at the Department of Electrical and Computer Engineering, Université Laval, Québec, QC, Canada. His research interests include photonic integrated circuit design, and simulation and characterization of space division multiplexing systems.

Zhongjin Lin was born in Zhanjiang, China, in 1992. He received his B.S. degree in Photoelectronic Science and Technology fromChangchun University of Science and Technology, Changchun, China in 2013. He is currently working toward his Ph.D. degree at the Department of Electrical and Computer Engineering, Universit Laval, Qubec, QC, Canada. His research interests include chip-scale polarization and spectrum analyzer, and the application of the nanoantennas.

Simon Bélanger-de Villers received the B. Eng. degree in engineering Physics from Universit Laval, Qubec, QC, Canada, in 2018, where he is currently working toward the M.Sc. degree in electrical engineering. His research is focused on integrated microring filters and modulators on silicon for telecommunications.

Leslie A. Rusch (S'91-M'94-SM'00-F'10) received the B.S.E.E. degree (with honors) from the California Institute of Technology, Pasadena, CA, USA, in 1980 and the M.A. and Ph.D. degrees in electrical engineering from Princeton University, Princeton, NJ, in 1992 and 1994, respectively. She holds a Canada Research Chair in *Communications Systems Enabling the Cloud*, is a full Professor in the ECE Department at Universit Laval, QC, Canada, where she is also a member of the Centre for Optics, Photonics, and Lasers (COPL). She has experience in defense, industrial, and academic communications research. She was a communications project engineer for the Department of Defense from 19801990. While on leave from Universit Laval, she spent two years (20012002) at Intel Labs creating and managing a group researching new wireless technologies. Prof. Rusch performs research on wireless and optical communications. Her research interests include digital signal processing for coherent detection in optical communications, spatial multiplexing using orbital angular momentum modes in fiber, radio over fiber, and OFDM for passive optical networks; and in wireless communications, optimization of the optical/wireless interface in emerging cloud based computing networks, and implantable medical sensors with high bit rate UWB telemetry. She is recipient of the IEEE Canada Fessenden Award for Telecommunications research, and the IEEE Canada J. M. Ham Award for Graduate Supervision. Prof. Rusch has published over 130 journal articles in international journals (90% IEEE/IEE) with wide readership, and contributed to over 165 conferences. Her articles have been cited over 5100 times per Google Scholar.

Wei Shi (S'07-M'12) is an Associate Professor in the Department of Electrical and Computer Engineering, Université Laval, Québec, QC, Canada. He received the Ph.D. degree in electrical and computer engineering from the University of British Columbia, Vancouver, BC, Canada, in 2012, where he was awarded the BCIC Innovation Scholarship for a collaboration entrepreneurship initiative. Before joining Universit Laval in 2013, he was a researcher at McGill University, Montreal, QC, Canada, where he held a Postdoctoral Fellowship from the Natural Sciences and Engineering Research Council of Canada (NSERC). He is currently an Associate Professor with the Department of Electrical and Computer Engineering, Université Laval, Québec, QC, Canada. His current research focuses on integrated photonic devices and systems, involving silicon photonics, nanophotonics, CMOS-photonics co-design, high-speed optical communications, chip-scale lasers, and optical sensors. He is a member of the Center for Optics, Photonics and Lasers (COPL) and holds a Canada Research Chair in Silicon Photonics.

National Science and Engineering Research Council of Canada (NSERC) Funding: CRDPJ 515539-17